

## RADAR REFRACTIVITY APPLICATIONS FOR CONVECTIVE INITIATION FORECASTING AND OBSERVATIONS OF THE CONVECTIVE BOUNDARY LAYER

D. Bodine<sup>1,2,\*</sup>, P. L. Heinselman<sup>3</sup>, B. L. Cheong<sup>2</sup>, R. D. Palmer<sup>1,2</sup>, and D. Michaud<sup>1,2</sup>

<sup>1</sup> School of Meteorology, The University of Oklahoma, Norman, OK, U.S.A.

<sup>2</sup> Atmospheric Radar Research Center, The University of Oklahoma, Norman, OK, U.S.A.

<sup>3</sup> Cooperative Institute of Mesoscale Meteorological Studies (CIMMS), The University of Oklahoma, Norman, OK, U.S.A.

### 1. INTRODUCTION

Quantitative precipitation forecasting (QPF) skill is very low during the warm season, when convective weather has the greatest impact on society (Uccellini et al. 1999; Fritsch and Carbone 2004). The absence of high-resolution water vapor measurements remains a major limitation for convective weather forecasting (Emanuel et al. 1995; Dabberdt and Schlatter 1996; National Research Council 1998). Convection initiation is often dependent on small-scale variations in moisture, and these variations cannot be resolved by the limited spatial resolution of the Automated Surface Observing System (ASOS). Thus, a major breakthrough in convective weather forecasting could result from improved near-surface moisture measurements.

Several modeling and observational studies have found that small-scale variations in moisture are often critical for convection initiation. Numerical simulations by Crook (1996) found that convection initiation was sensitive to small-scale variations in surface moisture. Ziegler et al. (1996), Ziegler and Rasmussen (1998), and Parsons et al. (2000) found that strong moisture gradients along the dryline were important for convection initiation, and Ziegler et al. (1996) suggested that observing *meso- $\gamma$*  (2–20 km) variations in moisture are critical for convection initiation forecasting.

Horizontal variations in moisture develop as boundary layer circulations transport moisture vertically. At small scales (3–6 km) (Stull 1988), horizontal moisture variations develop between updraft and downdraft branches of horizontal convective rolls (Weckwerth et al. 1996). The updraft branches of horizontal convective rolls are associated with increased moisture, and are often favorable regions for convection initiation, while the downdraft branches transport dry air above the capping inversion to the surface (Weckwerth et al. 1996). The variability of moisture at smaller scales may be further modulated by gravity waves (convection waves) above the horizontal convective rolls (Clark et al. 1986). The convection waves have wavelengths between 5 and 15 km (Kuettner et al. 1987), introducing larger scale moisture variability (Clark et al. 1986).

The relationship between small-scale moisture variability and convection initiation motivated the International H<sub>2</sub>O

Project (IHOP), which was designed to investigate of the spatial and temporal distribution of water vapor in the atmosphere, and assess its impact on convection initiation (Weckwerth et al. 2004). The dynamics of an active pre-convective environment containing: a dryline, outflow boundary, HCRs, internal gravity waves, were thoroughly analyzed for one IHOP case. However, the specific location of convection initiation could not be attributed to dynamics (Weckwerth et al. 2008). Weckwerth et al. (2008) suggested that while dynamical processes are important for convection initiation, small-scale moisture variations might be important to explain why convection initiation occurred at a particular location.

Radar refractivity retrievals (Fabry et al. 1997; Fabry 2004; Cheong et al. 2008) have shown promise in providing near-surface moisture measurements at much better spatial resolution than the ASOS network. Radar refractivity retrievals are obtained from ground clutter phase measurements, and provide refractivity data out to a range of approximately 50 km. The noisiness of phase measurements requires smoothing and interpolation, so the analyses in this study will use 4-km refractivity data. Given that the spatial resolution of radar refractivity data is 4 km, phenomena with wavelengths smaller than 8 km (Nyquist interval twice sampling resolution) may not be resolved because the smoothing acts as a low-pass filter. Thus, refractivity will show larger-scale organization of moisture and moisture change patterns in the convective boundary layer (CBL).

Refractivity is related to temperature, pressure and water vapor pressure using the following equation:

$$N = 77.6 \frac{p}{T} + 3.73 \times 10^5 \frac{e}{T^2} \quad (1)$$

where  $p$  is pressure in hPa,  $T$  is the temperature in Kelvin, and  $e$  is the water vapor pressure in hPa (Bean and Dutton 1968). At warmer temperatures, the variability of refractivity is primarily caused by water vapor because the contributions of temperature and pressure changes to refractivity are relatively small. Thus, refractivity fields can be used as a proxy for moisture near the surface. Several studies have demonstrated that moisture changes associated with cold fronts, outflow boundaries, drylines, boundary layer structures and other mesoscale phenomena can be observed by radar refractivity retrievals (Weckwerth et al. 2005; Fabry 2006; Demoz et al. 2006; Buban et al.

\* Corresponding author address: David Bodine, University of Oklahoma, School of Meteorology, 120 David L. Boren Blvd., Rm 4630, Norman, OK 73072-7307; e-mail: bodine@ou.edu

2007; Roberts et al. 2008; Bodine et al. 2008; Heinselman et al. 2008).

The capability of refractivity data to observe small-scale moisture changes that are often critical for convection initiation has been documented. During IHOP, the small-scale variability of moisture was analyzed using radar refractivity retrievals (Fabry 2006). Fabry (2006) found that moisture variability in the boundary layer increased as dry air from the inversion layer mixed with the top of the boundary layer. The study also showed that surface moisture variability could be calculated from the rate of entrainment of dry air. Using a combination of radar refractivity data and in-situ moisture measurements from aircraft, Fabry (2006) found that moisture variability had a greater effect on convective inhibition at smaller scales (less than 20 km) compared to temperature variability. While this study focused on statistical aspects of moisture on convection initiation, Bodine et al. (2008) presented a case where a small moisture pool in refractivity likely explained the specific location of convection initiation for an isolated storm.

The primary objectives of this study are to answer the following questions for the data examined:

- What spatial and temporal patterns in moisture are typical of the convective boundary layer?
- What processes instigate and modulate moisture variability in the convective boundary layer?

This study analyzes boundary layer moisture patterns for a two-month period in late spring and early summer in southwest Oklahoma using refractivity data from the Frederick, Oklahoma (KFDR) Weather Surveillance Radar-1988 Doppler radar (WSR-88D). Thunderstorms frequently develop in the late spring and early summer in southwest Oklahoma, so the moisture patterns analyzed in this study could be applied to convection initiation studies in the Great Plains. The first part of the study examines statistical aspects of moisture in the convective boundary layer, focusing on temporal and spatial variability of the drying and moistening rate and field movement. The second part of the study investigates two convective boundary layer cases. The first case shows the temporal evolution of moisture variability for a typical well-mixed boundary layer case. The second case demonstrates the capability of refractivity to detect moisture variations along a secondary boundary likely caused with mesocyclones.

## 2. EXPERIMENT CONFIGURATION

### 2a. Radiosonde data and CBL classification method

Radiosonde data from Norman, Oklahoma (OUN) was used to estimate the height of the bottom of the capping inversion,

and to calculate boundary layer and inversion layer mean quantities, including wind speed and direction, potential temperature gradients, vertical wind shear. The 0000 UTC OUN soundings were obtained from 24 May 2008 to 31 July 2008. The closest sounding launch site to KFDR was OUN, which is approximately 169 km from KFDR. Hence, it is assumed that the OUN sounding is representative of the KFDR site. In some cases where the conditions were significantly different, the sounding analysis was omitted.

The boundary layer depth was defined as the distance between the surface and the bottom of the inversion layer. The mean convective boundary layer wind speed and direction were calculated by weighting each sounding measurement by its depth ( $\Delta z$ ). To calculate the weight for each layer, ( $\Delta z$ ) was divided by the total depth of the boundary layer. To analyze CBL stability, the Richardson Number,  $Ri$ , was calculated using (2)

$$Ri = \frac{g \frac{\Delta \theta}{\bar{\theta} \Delta z}}{\left(\frac{|\Delta \vec{u}|}{\Delta z}\right)^2} \quad (2)$$

where  $\bar{\theta}$  is the mean potential temperature of the layer,  $\vec{u}$  is the horizontal wind vector, and  $g$  is the gravitational constant of acceleration. Weighted averages of  $\frac{\Delta \theta}{\Delta z}$  and  $\frac{|\Delta \vec{u}|}{\Delta z}$  were computed using the radiosonde potential temperature and wind measurements within the convective boundary layer. The mean mixing ratio for the boundary layer and inversion layer were also calculated using a weighted average based on ( $\Delta z$ ).

Based on the radiosonde data, each day was classified into two sets of cases: well-mixed convective boundary layer (WCBL) cases, and a poorly-mixed convective boundary layer cases (PCBL). The classification was based on the following criteria:

- $Ri < 1$
- $\frac{d\theta}{dz} < 1 \text{ K km}^{-1}$
- Inversion height  $> 1500 \text{ m}$

If at least two of the three criteria were met, then the day was classified as a WCBL case. Otherwise, the day was classified a PCBL case. The Richardson Number and vertical potential temperature gradient were used to evaluate the stability of the boundary layer, and the inversion height was used to assess how deeply the CBL was mixed. Typically,  $Ri < 0.25$  or  $\frac{d\theta}{dz} < 0 \text{ K km}^{-1}$  indicate neutral or unstable conditions observed in a well-mixed convective boundary layer (Stull 1988). The slightly higher Richardson Number and vertical potential temperature gradient were designed to account for stabilization of the lower boundary layer occurring in the early evening before the 0000 UTC sounding.

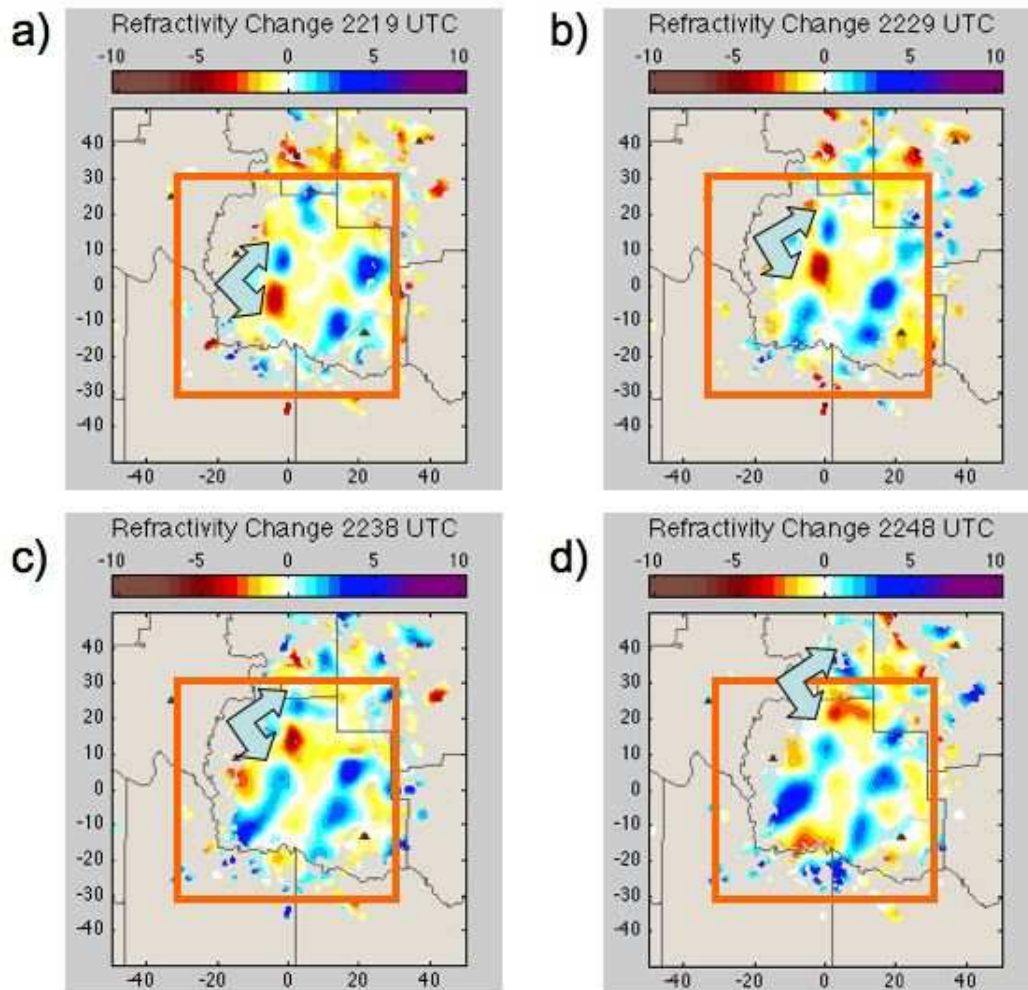


Figure 1: Plot of scan-to-scan refractivity at a) 2215, b) 2225, c) 2235, d) 2245 UTC on 3 June 2008. The orange box shows the analysis area for the cross-correlation analysis. The blue arrows point toward two coherent structures in the refractivity data moving northward.

The refractivity data analysis will focus on the WCBL cases to satisfy the objectives of the study. The PCBL (poorly-mixed convective boundary layer) cases were omitted from the study because large contributions of moisture variability were frequently observed that were not caused by boundary layer processes (e.g. moisture variability caused by precipitation, fronts, etc.). Thus, these cases would not be useful for a convective boundary layer study.

## 2b. Refractivity data analysis

**i. Data and post-processing** Radar refractivity data were collected from KFDR and the Oklahoma City, Oklahoma (KTLX) WSR-88Ds during the 2008 Spring Refractivity Experiment, which was designed to obtain forecaster evaluations of radar refractivity data (Heinselman et al. 2008). The algorithm used to obtain the radar refractivity retrievals was developed independently by the Atmospheric Radar Research Center (ARRC) at the University of Oklahoma (OU; Cheong et al. (2008)), based on Fabry et al. (1997) and Fabry (2004). The main differences between the OU algorithm (Cheong et al. 2008) and Fabry (2004) involve the processing of the data (e.g. smoothing), and using Mesonet observations to create a reference map. Cheong et al. (2008) provides a detailed description of the OU algorithm.

The KFDR refractivity data analyzed in this study were collected from 23 May 2008 to 30 July 2008, and KTLX refractivity data were analyzed for 21 April 2008. Owing to technical issues, KFDR refractivity data between 9 June and 24 June 2008 were unavailable. The three refractivity products analyzed in this study are absolute refractivity (hereafter called refractivity), scan-to-scan refractivity change (hereafter called scan-to-scan refractivity), and normalized scan-to-scan refractivity. Scan-to-scan refractivity is defined as the refractivity change between two volume scans (usually 5–10 minutes), and is more accurate than measurements of refractivity (Fabry 2006). Because different volume coverage patterns have different scan times, it is useful to normalize scan-to-scan refractivity. For this study, the scan-to-scan refractivity change was normalized to one hour, giving the product called normalized scan-to-scan refractivity.

Both ungridded (raw) and gridded refractivity data were used to analyze the spatial and temporal variability of refractivity and scan-to-scan refractivity. The ungridded data were used to calculate spatial means and standard deviations of the refractivity and scan-to-scan refractivity fields. The gridded data were used to compute field movement speed. The refractivity data were converted from polar to Cartesian coordinates and then gridded to a 0.5 by 0.5 km grid using nearest-neighbor interpolation. Given that refractivity retrievals near the edge of the domain can be noisy and

discontinuous owing to greater spacing between clutter targets, a 60 km by 60 km subsection of the refractivity field, centered on the radar, was selected for analysis (Fig. 1). Within this smaller domain, the clutter targets are closely spaced, providing higher accuracy of refractivity measurements.

**ii. Spatial and Temporal Variability Analysis** To study the temporal evolution of moisture in the well-mixed convective boundary layer, study-long, hourly averages of scan-to-scan and normalized scan-to-scan refractivity change were calculated. Scan-to-scan refractivity measures short-term moisture changes, and normalized scan-to-scan refractivity measures rate of moisture change.

For each volume scan, the mean volume-scan scan-to-scan refractivity was computed by averaging all of the range gates for each field, using

$$\overline{SS} = \frac{\sum_{i=1}^N SS_i}{N} \quad (3)$$

where  $\overline{SS}$  is the mean volume-scan scan-to-scan refractivity,  $N$  is the number of gates, and  $SS_i$  is the scan-to-scan refractivity measurement at gate  $i$ . Similarly, the mean volume-scan normalized scan-to-scan refractivity was computed by averaging all of the normalized scan-to-scan refractivity measurements for each gate. Then, one-hour averages of scan-to-scan refractivity were computed using all of the volume scans during each one-hour period, using

$$\overline{SS}_{j,k}^{hr} = \frac{\sum_{i=1}^M \overline{SS}_i}{M} \quad (4)$$

where  $\overline{SS}_{j,k}^{hr}$  is the one-hour average of scan-to-scan refractivity for hour  $j$  and WCBL case  $k$ .  $M$  is the number of scans during the one-hour period, and  $\overline{SS}_i$  is the individual mean volume-scan scan-to-scan refractivity for scan  $i$ . Similarly, the one-hour average of normalized scan-to-scan refractivity was computed by averaging the mean volume-scan normalized scan-to-scan refractivity for the  $M$  volume scans during the one-hour period.

To develop a climatology of the temporal evolution of well-mixed convective boundary layer cases between 1400 and 0000 UTC, the study-long, hourly scan-to-scan refractivity mean,  $\overline{SS}_{j,k}^{hr}$ , was calculated using

$$\overline{\overline{SS}}_j = \sum_{k=1}^{23} \frac{\sum_{i=1}^N \overline{SS}_{j,k}^{hr}}{N} \quad (5)$$

where  $\overline{\overline{SS}}_j$  is the study-long hourly average of scan-to-scan refractivity for the one-hour period,  $j$ , for  $N$  WCBL cases.  $\overline{SS}_{j,k}^{hr}$  is the one-hour average of scan-to-scan refractivity for hour,  $j$ , and case  $k$ . Similarly, the study-long, hourly mean of normalized scan-to-scan refractivity was calculated

by averaging the individual one-hour averages of normalized scan-to-scan refractivity for each WCBL case. Additionally, the median study-long, hourly median of scan-to-scan and normalized scan-to-scan refractivity were computed to reduce the effects of outliers with the relatively small data set. The study-long hourly medians of scan-to-scan and normalized scan-to-scan refractivity were computed using the one-hour averages of scan-to-scan and normalized scan-to-scan refractivity from each WCBL case.

To develop a climatology of spatial variability of moisture and short-term moisture changes, study-long, hourly averages of the standard deviation of refractivity and scan-to-scan refractivity were computed. Volume scan standard deviations were calculated for refractivity and scan-to-scan refractivity, similar to (3). Then, one-hour averages of standard deviation were computed using all of the volume-scan standard deviations within the one-hour period, similar to (4). Using the one-hour averages from each WCBL, the study-long, hourly average standard deviation of refractivity and scan-to-scan refractivity were computed, similar to (5).

**iii. Field movement analysis** Wave-like refractivity structures were frequently observed in refractivity and exhibited temporal continuity between scans (Fig. 1). The cross-correlation analyses were used to study the movement of wave-like refractivity structures. Cross-correlation analyses have been used for storm tracking (Rinehart and Garvey 1978) and tracking boundary layer echoes (Tuttle and Foote 1990) to determine storm or boundary layer movement.

Before the cross-correlation was calculated, the two-dimensional spatial mean of the gridded scan-to-scan refractivity field was computed. Then, the perturbation scan-to-scan refractivity field was obtained by subtracting the spatial mean from the gridded scan-to-scan refractivity data. To obtain the field movement speed, the perturbation scan-to-scan refractivity fields from two consecutive volume scans were used, at times  $t_1$  and  $t_0$ . The two-dimensional cross-correlation was computed using

$$B(i, j) = \sum_{m=0}^{M-1} \sum_{n=0}^{N-1} A_1(m, n) * \text{conj}(A_0(m+i, n+j)) \quad (6)$$

where  $B(i, j)$  is the cross-correlation evaluated at point  $i$  and  $j$ , matrices  $A_1$  and  $A_0$  represent the perturbation scan-to-scan refractivity fields at times  $t_1$  and  $t_0$ , respectively, and  $M$  and  $N$  are the dimensions of  $A_1$  (same as  $A_0$ ).

After the cross-correlation was computed, the maximum correlation of the cross-correlation analysis was located. The location of the maximum correlation ( $i_{max}, j_{max}$ ) of the cross-correlation corresponds to the position where the matrices have the most similar structure, i.e. the new position of the field. The center of  $B$  is the original position of the field ( $i_0, j_0$ ) at time  $t_0$ . A translation vector  $\vec{d}$  can be

defined as the displacement between times  $t_1$  and  $t_0$ , using

$$\vec{d} = [(i_{max} - i_0)\hat{i} + (j_{max} - j_0)\hat{j}] * \Delta_{grid} \quad (7)$$

where  $\Delta_{grid}$  is the grid spacing, 0.5 km. The field movement speed,  $\vec{v}$ , can then be obtained by dividing the displacement vector,  $\vec{d}$ , by the time between volume scans.

The mean cross-correlation estimated field movement was calculated for each WCBL case using the individual cross-correlation estimates from each scan between 2000 and 0000 UTC. High estimates of the field velocity occurred frequently because the periodic nature of the perturbation scan-to-scan refractivity field allows the field to be well-correlated at multiple locations, resulting in large displacements from the original position of the field. To eliminate high estimates of the field movement, all estimates outside two standard deviations of the median were removed.

## 2c. Surface data

Throughout the study, comparisons of the Oklahoma Mesonet and refractivity data verified the accuracy of the refractivity data and resolved any ambiguities of the contributions of vapor pressure, temperature and pressure to refractivity. The Oklahoma Mesonet provides reliable surface measurements every 5 min., with approximately 35-km spatial resolution (Brock et al. 1995; McPherson et al. 2007). 1.5 and 9 m temperature, dewpoint temperature, 2 and 10 m wind speed and direction, solar radiation and pressure data were obtained from the Oklahoma Mesonet. To compare the field movement to the surface wind, the mean surface 10 m wind speed and direction was computed from 2000 to 0000 UTC for each WCBL case. To analyze surface layer stability, the mean Richardson Number,  $Ri$ , was also computed for each WCBL case using Oklahoma Mesonet data (hereafter called Mesonet data) from 2000 to 0000 UTC.

## 3. BOUNDARY LAYER MOISTURE CLIMATOLOGY

During the analysis period, there were 54 afternoons (1400 to 0000 UTC) when refractivity data were collected. Based on the classification method presented in Section 2a, the 54 cases were classified as well-mixed convective boundary layer (WCBL) or poorly-mixed convective boundary layer (PCBL) cases based on the 0000 UTC OUN soundings. There were 32 WCBL (well-mixed convective boundary layer) and 22 PCBL (poorly-mixed boundary layer) cases. This climatology will focus on the convective well-mixed boundary layer (WCBL) cases.

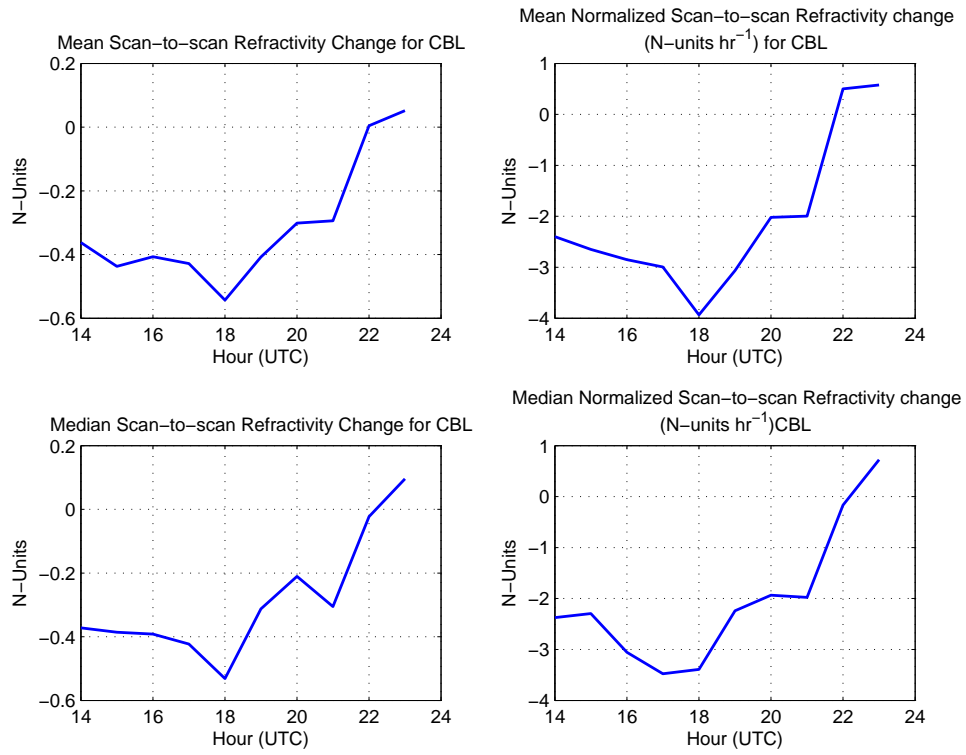


Figure 2: Mean and median hourly scan-to-scan (N-units) and normalized scan-to-scan refractivity change (N-units hr<sup>-1</sup>).

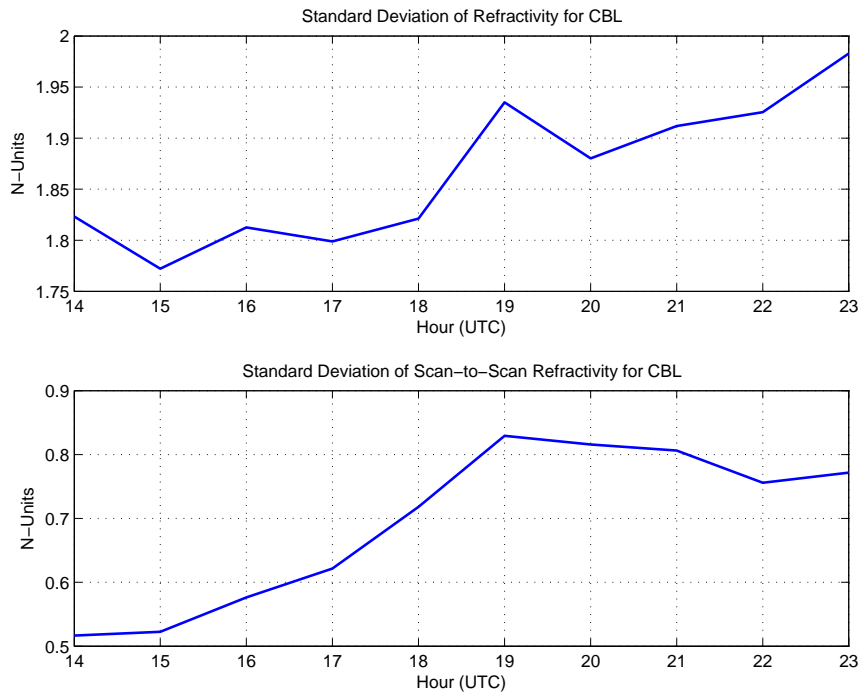


Figure 3: Mean standard deviation of refractivity and scan-to-scan refractivity for each one hour period from 1400 to 2300 UTC for all convective boundary layer cases.

### 3a. Temporal and Spatial Moisture Variability

The net moisture change in the boundary layer primarily results from dry air entrainment and surface moisture fluxes. Drying in the boundary layer occurs in the afternoon as the boundary layer grows and dry air is entrained from the capping inversion layer (Stull 1988; Fabry 2006). Surface moisture fluxes increase moisture near the surface, counteracting the drying caused by entrainment. The evolution of refractivity changes observed during the WCBL cases were consistent with the conceptual model of the well-mixed boundary layer.

The mean and median scan-to-scan refractivity changes were small, and negative (Fig. 2). Although the scan-to-scan refractivity changes were relatively small, over longer periods the accumulated change becomes significant. Using normalized scan-to-scan refractivity, the significance of the change becomes more evident. The mean and median normalized scan-to-scan refractivity changes were negative between 1400 and 2200 UTC, indicating drying throughout the afternoon (Fig. 2).

Based on the temporal evolution of the moisture changes shown in Figure 2, the contribution of dry air entrainment to moisture change,  $\frac{dq_{ent}}{dt}$ , exceeded the contribution of surface moisture fluxes,  $\frac{dq_{flux}}{dt}$ , leading to drying near the surface between 1400 and 2200 UTC. The greatest difference between  $\frac{dq_{ent}}{dt}$  and  $\frac{dq_{flux}}{dt}$  likely occurred between 1700 and 1800 UTC when the maximum drying rate was observed. The maximum mean and median drying rate were slightly greater than 3 N-units  $\text{hr}^{-1}$ , occurring at 1800 and 1700 UTC, respectively. From 1800 to 2200 UTC, the drying rate decreases as the contribution of dry air entrainment to moisture change decreases.

At approximately 2200 UTC, the surface moisture fluxes likely exceeded the moisture change caused by entrainment of dry air ( $\frac{dq_{flux}}{dt} > \frac{dq_{ent}}{dt}$ ), whereas before 2200 UTC the moisture change caused by entrainment of dry air likely exceeded the surface moisture flux ( $\frac{dq_{flux}}{dt} < \frac{dq_{ent}}{dt}$ ). The transition around 2200 UTC when  $\frac{dq_{flux}}{dt} > \frac{dq_{ent}}{dt}$  will be called the Late Afternoon Moisture Transition (LAMT). Using normalized scan-to-scan refractivity, the Late Afternoon Moisture Transition is defined at the time after which the normalized scan-to-scan refractivity remains positive. The Late Afternoon Moisture Transition is unrelated to the early evening transition (Acevedo and Fitzjarrald 2001), which occurs as the boundary layer decouples after sunset.

To analyze the spatial variability of moisture and drying rate, the hourly mean standard deviation of scan-to-scan refractivity and refractivity were calculated (Section 2bii). While these quantities may seem very similar, they measure different characteristics of the moisture field. For example, for a stationary, temporally invariant dryline, the standard

deviation of scan-to-scan refractivity would be zero because no temporal moisture changes would be occurring. However, the standard deviation of refractivity would be large owing to the large spatial gradients in moisture. In summary, the standard deviation of refractivity reflects the spatial moisture variability, and the standard deviation of scan-to-scan refractivity reflects the spatial variability of short-term moisture changes.

The mean standard deviation of refractivity increased between 1400 and 2300 UTC (Fig. 3), indicating an increase in moisture variability throughout the afternoon. The mean standard deviation for scan-to-scan refractivity approached a maximum at 1900 UTC, and remained nearly constant at 0.8 N-units until 2300 UTC (Fig. 3). This suggests an increase in the variability of short-term moisture changes through 1900 UTC, followed by relatively constant short-term moisture changes after 1900 UTC. The increase in variability of short-term moisture changes in the afternoon likely arises from modulation of moisture by boundary layer circulations, such as horizontal convective rolls.

### 3b. Field movement

The cross-correlation method described in section 2biii was used to calculate the mean motion of the moisture field. Temporally coherent, wave-like structures in the scan-to-scan refractivity field were frequently observed between 2000 and 0000 UTC, so the cross-correlation analysis focuses on this period. The mean cross-correlation velocity and mean Mesonet wind speed and direction were calculated for 2000 to 0000 UTC for each case, from 23 May 2008 to 9 June 2008. This period was selected for the analysis because it was relatively free of precipitation, and 16 of the 18 cases were classified as WCBL cases.

After removing poor cross-correlation estimates and poorly representative sounding observations, the correlation coefficients and biases were calculated for the mean cross-correlation velocity and the mean surface wind (10 m Mesonet wind), and for the mean cross-correlation velocity and the mean boundary layer wind. Generally, the mean surface wind and mean boundary layer wind show good agreement with the cross-correlation velocity (Fig. 4). For the mean surface wind and cross-correlation estimated velocity, the correlation coefficients for wind speed and direction were  $r=0.790$  and  $0.954$ , respectively. The mean biases for the cross-correlation estimated velocity and the mean surface wind speed and direction were  $4.54 \text{ ms}^{-1}$  and  $7.61^\circ$ , respectively. For the mean boundary layer wind and the cross-correlation estimated velocity, the correlation coefficient for wind speed and direction were  $r=0.817$  and  $0.959$ , respectively. The mean biases for the cross-correlation estimate and the mean boundary layer wind speed and direction were  $2.19 \text{ ms}^{-1}$  and  $5.6^\circ$ , respectively.

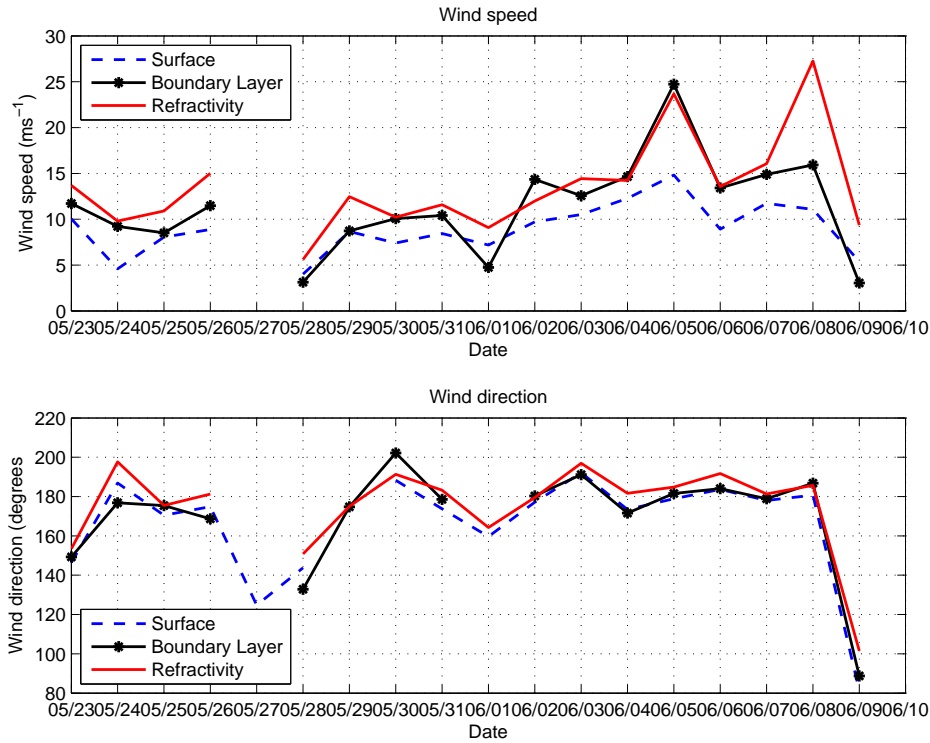


Figure 4: Afternoon (2000-0000 UTC) averages of Mesonet and boundary layer wind speed and direction, and cross-correlation (refractivity) velocity for 23 May 2008 to 9 June 2008.

Thus, the field movement estimated by the cross-correlation method agrees best with the mean convective boundary layer wind. The positive bias in wind speed can be explained by outliers in the cross-correlation velocity estimates.

#### 4. CASE STUDIES

##### 4a. Well-developed Boundary Layer Case - 3 June 2008

The moisture variability observed on 3 June 2008 was typical of convective boundary layer cases from the study. The 0000 UTC 4 June 2008 sounding (not shown) showed a deep stable layer above the CBL, extending from approximately 831 to 774 hPa. From the bottom to the top of the stable layer, the mixing ratio decreased from 12.1 to 5.7 g kg<sup>-1</sup>. The CBL was approximately neutral, with a 1.1 K increase in potential temperature from 345 to 1425 m. The Mesonet data also confirmed that the surface layer was approximately neutral, with a mean Ri of -0.05. Solar radiation data from the Mesonet showed that cloud cover was minimal until 2000 UTC and increased through 0000 UTC. Thus, given neutral conditions and a Ri near zero, the boundary layer was well-mixed throughout the afternoon. Between 1400 and 0000 UTC, the mean surface dewpoint temperature within the refractivity domain decreased from

20.0 to 15.1°C, and the standard deviation increased from 0.6 to 1.8°C. The Mesonet moisture measurements show that significant drying occurred near the surface and surface moisture variability increased throughout the day.

The spatial variability of short-term moisture changes was smallest during the morning. At 1501 UTC, scan-to-scan refractivity data showed fairly spatially uniform scan-to-scan refractivity changes, ranging from 0 to -1 N-units over 10 minutes (Fig. 6a). The mean normalized scan-to-scan refractivity change was greater than -5 N-units hr<sup>-1</sup> (Fig. 5b), relatively high compared to the daytime average (1400 to 0000 UTC). However, the temperature change was approximately 2°C hr<sup>-1</sup>, which corresponds to a decrease of approximately 2 N-units hr<sup>-1</sup>. Thus, the contribution of moisture to refractivity was only -3 N-units hr<sup>-1</sup>. The standard deviation of scan-to-scan refractivity was near a daytime minimum of 0.5 N-units, confirming the small spatial variability of short-term moisture changes (Fig. 5d). At 1501 UTC, the standard deviation of refractivity was at a local maximum of 2.5 N-units, owing to a southwest-northeast oriented refractivity gradient. The moisture gradient was caused by horizontal variations in mixing. Before 1501 UTC, the southwestern region of the refractivity field had experienced more mixing and drying compared to the northeastern region. The refractivity gradient persisted until

about 1700 UTC as the drier air mixed eastward, resulting in a more homogeneous refractivity field.

As the boundary layer continued to grow, evidence of boundary layer circulations affecting the moisture field emerged. By 1806 UTC, small pools of positive scan-to-scan refractivity change were observed in the refractivity field within the areas of negative scan-to-scan refractivity change (Fig. 6b). The positive and negative changes may reflect the transport of moisture by boundary layer circulations. The presence of boundary layer circulations might also be reflected in the standard deviation of scan-to-scan refractivity, which increased to approximately 0.8 N-units (Fig. 5d). The standard deviation of refractivity also increased as a west-east oriented gradient developed in refractivity.

The peak drying rate occurred at 2013 UTC, with a normalized scan-to-scan refractivity change of  $-8$  N-units  $\text{hr}^{-1}$  (Fig. 5b). The contribution of temperature to refractivity change was relatively small at 2013 UTC, so an 8 N-unit  $\text{hr}^{-1}$  drying rate is approximately equivalent to a  $-1.3^\circ\text{C hr}^{-1}$  in rate of dewpoint temperature change. The peak drying rate occurred later than the mean and median peak drying rates for all WCBL cases (Fig. 2).

The variability of short-term moisture changes continued to increase throughout the day. By 2101 UTC, the small pools of positive scan-to-scan refractivity changes increased in areal coverage (Fig. 6c). The standard deviation of the scan-to-scan refractivity was 1.1 N-units, also indicating an increase in variability of short-term moisture changes (Fig. 5d). The west-east oriented moisture gradient continued to persist, although slightly weaker than the gradient observed at 1806 UTC.

The Late Afternoon Moisture Transition occurred at 2230 UTC, later than the mean LAMT time of 2200 UTC for all WCBL cases. Given the very dry stable layer above the boundary layer, substantial dry air entrainment could occur in the boundary layer even after heating and boundary layer growth reduced in the late afternoon. Thus, drying could continue to occur in the boundary layer, hence the later LAMT.

After the Late Afternoon Moisture Transition, the areal coverage of small pools of positive scan-to-scan refractivity changes continued to increase in areal coverage and exhibited larger scale organization. At 2258 UTC, the small moisture pools were organized into bands with significant along-band variations in scan-to-scan refractivity (Fig. 6d). The individual pools of positive scan-to-scan refractivity within the band were observed moving north (Fig. 1), and displayed good temporal continuity between scans. The variability of short-term moisture changes reached a maximum of 1.8 N-units at approximately 2300 UTC. The higher moisture variability can be attributed to the

larger-scale organization of moisture patterns into bands, and increased small-scale variability within the large-scale bands.

#### 4b. Misocyclones

Misocyclones are vertically oriented vortices that are typically 0.5 to 2 km wide (Marquis et al. 2007). The development of misocyclones can occur as horizontal convective rolls are tilted upward by a boundary, such as a dryline (Buban et al. 2007). Misocyclones enhance convergence, leading to increased vertical velocities and increased moisture, which are favorable for convection initiation (Lee et al. 2000). The convergence pattern along a boundary with misocyclones follows a staircase pattern in reflectivity (Marquis et al. 2007).

On 21 April 2008, a double-dryline structure was observed near Oklahoma City, Oklahoma. Between 2000 and 2215 UTC, radar refractivity showed a tightening moisture gradient east of the dryline as a secondary boundary was developing. By 2215 UTC, a fine line appeared in the  $0.5^\circ$  reflectivity field along the secondary boundary, although the fine line was still partially obscured by the clutter field (Bodine et al. 2008). Large along-boundary variability in scan-to-scan refractivity was observed on 21 April 2008. Embedded regions of greater positive scan-to-scan refractivity change, which imply higher moisture change, were observed along the secondary boundary (Fig. 7 - 2225, 2234, 2244, 2254 UTC). As the fine line became better defined, a staircase pattern appeared in reflectivity along the secondary boundary (Fig. 7 - 2244, 2254 UTC), indicating the presence of misocyclones.

With horizontal convective rolls prominent in  $0.5^\circ$  reflectivity, this suggests the possibility of misocyclones at the intersection of the upward branch of the HCRs and the secondary boundary. Based on radar reflectivity, the approximate wavelength of the horizontal convective rolls,  $\lambda_{HCR}$ , was 5 km. The spacing of misocyclones along the boundary,  $\lambda_B$ , is determined by the wavelength of the horizontal convective rolls along the boundary, and the angle,  $\theta$ , between the HCRs and the boundary, as shown in equation (8).

$$\lambda_B = \frac{\lambda_{HCR}}{\sin(\theta)} \quad (8)$$

The wavelength between the embedded regions of higher moisture was approximately 9 km at 2225 and 2234 UTC, and approximately 12 km at 2245 and 2255 UTC (Fig. 7). The calculated spacing of misocyclones along the boundary was 10 km at 2225 and 2234 UTC. The increase in wavelength of the misocyclones between 2225 and 2254 UTC may be attributed to a decrease in angle between the HCRs and the boundary, or caused by a transition to mesoscale dryline waves (Koch and McCarthy 1982; McCarthy and Koch 1982) as the secondary

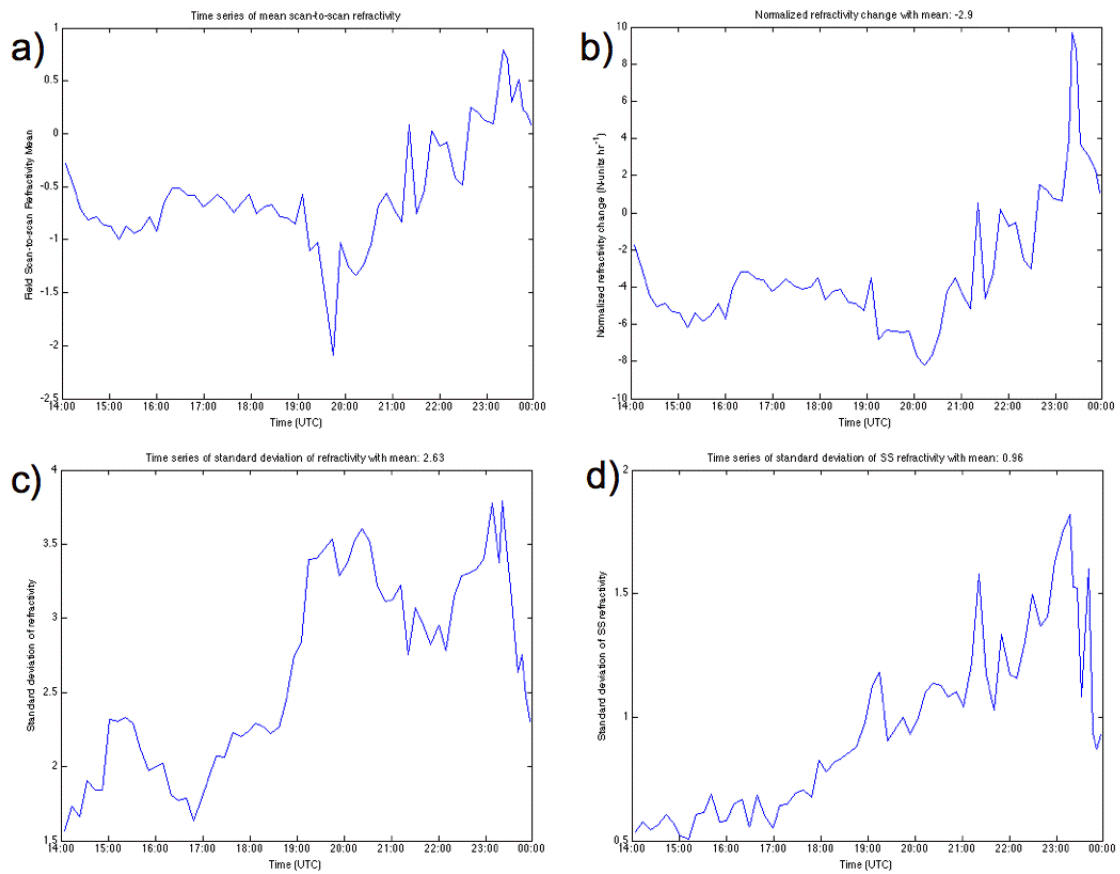


Figure 5: Time series plots of a) scan-to-scan refractivity b) normalized scan-to-scan refractivity c) standard deviation of refractivity d) standard deviation of scan-to-scan refractivity on 3 June 2008.

boundary retrograded. The HCRs were moving eastward at approximately  $5 \text{ m s}^{-1}$ , which corresponds to a movement of  $10.4 \text{ m s}^{-1}$  to the north along the boundary, and the approximated speed of the misocyclones along the boundary was  $8.3 \text{ m s}^{-1}$ . Thus, the northward movement also corroborates the presence of misocyclones along the secondary boundary.

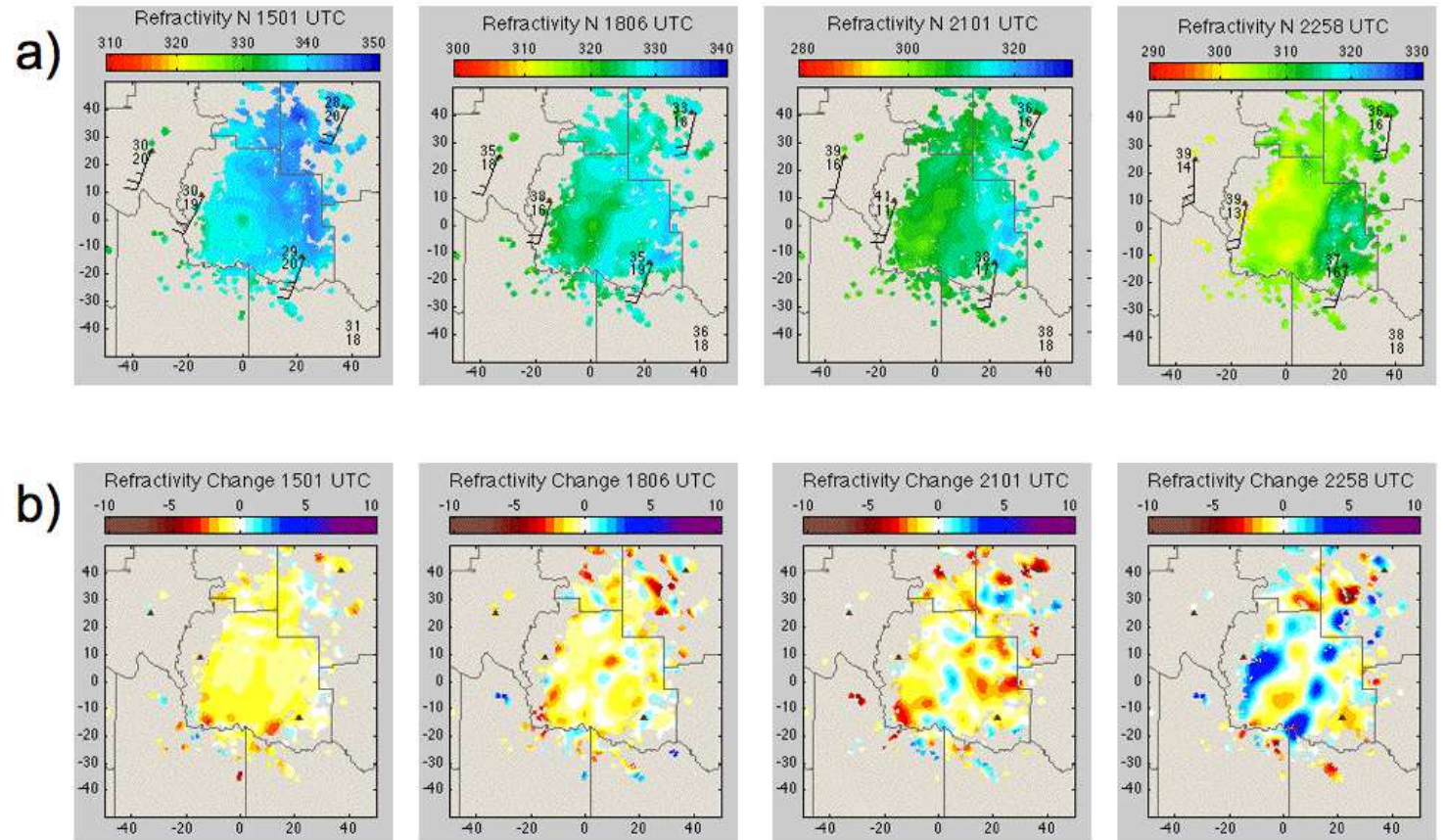


Figure 6: KFDR a) refractivity and b) scan-to-scan refractivity at 1501 UTC, 1806 UTC, 2101 UTC, and 2258 UTC on 3 June 2008.

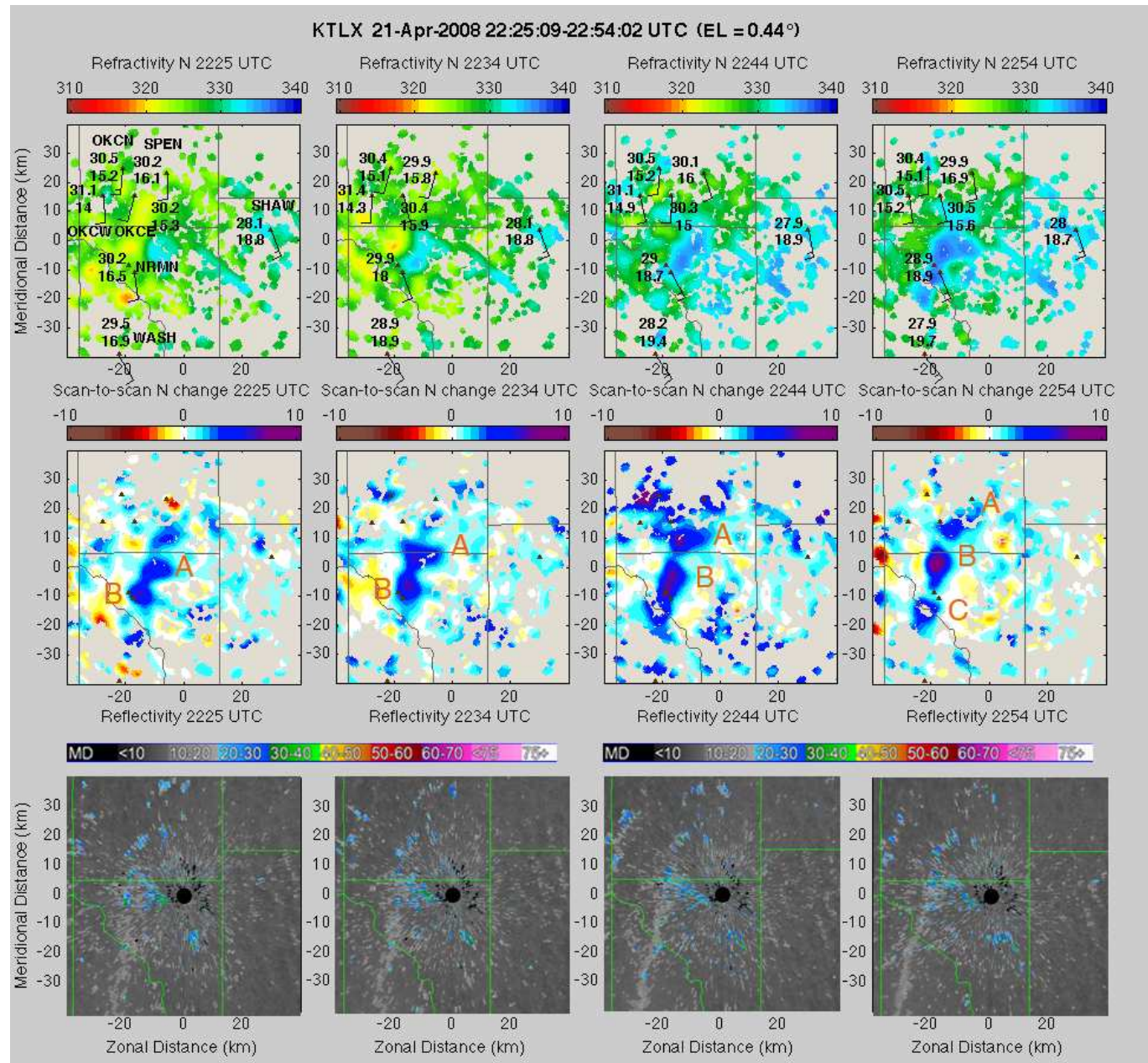


Figure 7: Refractivity, scan-to-scan refractivity, and reflectivity at 2225, 2234, 2244, 2254 UTC on 21 April 2008. The embedded positive moisture perturbations along the boundary are labelled A, B, and C. Note the northward progression of the individual moisture perturbations.

## 5. DISCUSSION

### 5a. *Modulation of Boundary Layer Moisture*

The cross-correlation analyses showed that short-term moisture changes in the CBL approximately move at the mean boundary layer wind speed. This result implies that the near-surface moisture field is impacted by moisture changes throughout the boundary layer. Furthermore, the cross-correlation analysis implies two possible results: (i) moisture is advected by the mean CBL wind by stationary CBL circulations, or (ii) changes in moisture are caused by CBL circulations that move at the mean CBL wind speed. Convection waves could cause along-wind modulation of boundary layer moisture observed in the 3 June 2008 case and days included in this study. Convection waves typically possess wavelengths of 5 to 15 km, and have been documented to move at the mean CBL wind speed (Kuettner et al. 1987). The nonlinear interaction between convection waves and convective boundary layer circulations, such as horizontal convective rolls or cellular convection, can further modulate convective boundary layer circulations and moisture perturbations produced by the boundary layer circulations (Balaji and Clark 1988). Thus, the modulation of the moisture field by convection waves could explain result (ii).

### 5b. *Impact on convection initiation*

The 3 June 2008 case study, which was typical of well-mixed CBL cases, showed that moisture variability and variability of short-term moisture changes increased throughout the day. During the late afternoon and early evening, the increased moisture variability implies a higher variability of convective inhibition (CIN) and convective available potential energy (CAPE). Convection initiation is sensitive to variations in CAPE and especially CIN, thus resolving variations in moisture is important for convection initiation forecasting. The 3 June 2008 case showed a larger scale organization of moisture patterns into moist bands during the late afternoon when convection initiation frequently occurs. The regions of positive scan-to-scan refractivity change (increase in moisture) may also be favorable for convection initiation, where moist regions in roll circulations or convection waves in the CBL are co-located with enhanced vertical motion. Furthermore, variability along the moist bands observed in refractivity suggests that convection initiation may be further tied to regions of enhanced moisture within the bands, which may also be co-located with stronger updrafts.

## 6. CONCLUSIONS

Radar refractivity fields provide a high-resolution, two-dimensional view of near-surface moisture. The study investigated afternoon moisture variability between 1400 and 0000 UTC for 32 WCBL cases. Based on the study-long, hourly mean normalized scan-to-scan refractivity, drying was observed between 1400 and 2200 UTC as moisture changes caused by entrainment likely exceeded moisture changes caused by surface moisture fluxes. The peak drying rate typically occurred between 1700 and 1900 UTC, and was approximately  $-3$  N-units  $\text{hr}^{-1}$ . After 1900 UTC, the drying rate decreased until the Late Afternoon Moisture Transition. The Late Afternoon Moisture Transition occurred when the net moisture change became positive, likely because moisture changes caused by moisture fluxes exceeded moisture changes caused by entrainment.

Refractivity data showed that the spatial variability of moisture and short-term moisture changes increased through 1900 UTC, and remained approximately constant through 0000 UTC. The increased variability of short-term moisture changes is likely caused by boundary layer circulations. The cross-correlation analysis agreed well with the mean CBL wind, suggesting that the moisture field is either advected by the CBL wind, or modulated by CBL circulations that move with the mean CBL wind.

The two case studies demonstrated the capability of refractivity to observe larger scale organization (10-20 km) of moisture patterns. The evolution of moisture variability and variability of short-term moisture changes from the 3 June 2008 case was similar to moisture variability and variability of short-term moisture changes observed throughout the study. The 3 June 2008 case showed that the coherent structures increased in wavelength in the late afternoon, and evolved into moist bands oriented approximately along-wind. Significant along-band moisture variability was also observed. The 21 April 2008 case also demonstrated the capability to use refractivity to detect enhanced moisture pools likely caused by misocyclones along a secondary dryline. Misocyclones likely caused significant along-boundary variations in moisture as the secondary boundary moved westward.

The results from this study suggest that refractivity could be useful for convection initiation forecasts. The cross-correlation analysis showed the capability of refractivity data to detect and track moisture perturbations caused by coherent CBL structures. These moisture perturbations cause variability in CIN and CAPE, which affect the likelihood of convection initiation. Thus, data assimilation of refractivity data could improve convection initiation forecasts because radar refractivity data can detect moisture perturbations associated with boundary layer circulations, misocyclones or

mesoscale dryline waves that would not be resolved by the ASOS network.

The Atmospheric Radar Research Center at the University of Oklahoma (OU) has developed the largest refractivity network with a seven-radar network of Doppler radars collecting radar refractivity data, providing a nearly complete swath of moisture measurements in southwest Oklahoma. Radar refractivity experiments at OU will continue through 2010 with an emphasis on studying convection initiation and data assimilation of refractivity data. The framework for refractivity data assimilation has been developed by the Center for Analysis and Prediction of Storms (Shimose et al. 2009). Shimose et al. (2009) showed that assimilation of simulated phase difference fields (closely related to refractivity) positively impacted the estimates of the near-surface moisture field.

## 7. ACKNOWLEDGMENTS

Funding for this research was provided by the Radar Operations Center through grant number NA17RJ1227 and the National Science Foundation through grant number ATM0750790. The first author was supported by an American Meteorological Society Fellowship sponsored by the Raytheon Corporation. The authors would like to thank the Radar Operations Center for maintaining the data flow from KTLX and KFDR during the experiments. The authors would also like to thank Kevin Manross, Travis Smith, and Brad Isom for their assistance. Finally, the authors would like to thank Conrad Ziegler for comments on a section of the paper.

## References

- Acevedo, O. C. and D. R. Fitzjarrald, 2001: The early evening surface-layer transition. *J. Atmos. Sci.*, **58**, 2650–2667.
- Balaji, V. and T. L. Clark, 1988: Scale selection in locally forced convective fields and the initiation of deep cumulus. *J. Atmos. Sci.*, **45**, 3188–3211.
- Bean, B. R. and E. J. Dutton, 1968: *Radio Meteorology*. Dover Publications, 435 pp.
- Bodine, D., P. L. Heinselman, B. L. Cheong, R. D. Palmer, and D. Michaud, 2008: Convection initiation and storm evolution forecasting applications of radar refractivity retrievals. *Wea. Forecasting*, submitted.
- Brock, F. V., K. C. Crawford, R. L. Elliott, G. W. Cuperus, S. J. Stadler, H. L. Johnson, and M. D. Eilts, 1995: The Oklahoma Mesonet: A technical overview. *J. Atmos. Oceanic Technol.*, **12**, 5–19.
- Buban, M., C. Ziegler, E. Rasmussen, and Y. Richardson, 2007: The dryline on 22 May 2002 during IHOP: Ground-radar and in situ data analyses of the dryline and boundary layer evolution. *Mon. Wea. Rev.*, **135**, 2473–2505.
- Cheong, B. L., R. D. Palmer, C. D. Curtis, T.-Y. Yu, D. S. Zrnić, and D. Forsyth, 2008: Refractivity retrieval using the Phased Array Radar: First results and potential for multi-function operation. *IEEE Tran. Geosci. Remote Sensi.*, **46**, 2527–2537.
- Clark, T. L., T. Hauf, and J. P. Kuettnner, 1986: Convectively forced internal gravity waves: Results from two-dimensional numerical experiments. *Quart. J. Roy. Meteor. Soc. J.*, **112**, 899–925.
- Crook, A. N., 1996: Sensitivity of moist convection forced by boundary layer processes to low-level thermodynamic fields. *Mon. Wea. Rev.*, **124**, 1767–1785.
- Dabberdt, W. F. and T. W. Schlatter, 1996: Research opportunities from emerging atmospheric observing and modeling capabilities. *Bull. Amer. Meteor. Sci.*, **77**, 305–323.
- Demoz, B., C. Flamant, T. Weckwerth, D. Whiteman, K. Evans, F. Fabry, P. Girolamo, D. Miller, B. Geerts, W. Brown, G. Schwemmer, B. Gentry, W. Feltz, and Z. Wang, 2006: The dryline on 22 May 2002 during IHOP: Convective-scale measurements at the profiling site. *Mon. Wea. Rev.*, **134**, 294–310.
- Emanuel, K., K. D. Raymond, A. Betts, L. Bosart, C. Bretherton, K. Droegemeier, B. Farrell, J. M. Fritsch, R. Houze, M. LeMone, D. Lilly, R. Rotunno, M. Shapiro, R. Smith, and A. Thorpe, 1995: Report of first prospectus development team of the U.S. weather research program to NOAA and the NSF. *Bull. Amer. Meteor. Sci.*, **76**, 1194–1208.
- Fabry, F., 2004: Meteorological value of ground target measurements by radar. *J. Atmos. Oceanic Technol.*, **21**, 560–573.
- 2006: The spatial variability of moisture in the boundary layer and its effect on convective initiation: Project-long characterization. *Mon. Wea. Rev.*, **134**, 79–91.
- Fabry, F., C. Frush, I. Zawadzki, and A. Kilambi, 1997: On the extraction of near-surface index of refraction using radar phase measurements from ground targets. *J. Atmos. Oceanic Technol.*, **14**, 978–987.
- Fritsch, J. M. and R. E. Carbone, 2004: Improving quantitative precipitation forecasts in the warm season: A USWRP research and development strategy. *Bull. Amer. Meteor. Sci.*, **85**, 955–966.

- Heinselman, P. L., B. L. Cheong, R. D. Palmer, D. Bodine, and K. Hondl, 2008: Radar refractivity retrievals from KTLX: Insights into operational benefits and limitations. *Wea. Forecasting*, Submitted.
- Koch, S. E. and J. McCarthy, 1982: The evolution of an Oklahoma dryline. part II: Boundary-layer forcing of mesoconvective systems. *J. Atmos. Sci.*, **39**.
- Kuettner, J., P. A. Hildebrand, and T. L. Clark, 1987: Observations of gravity wave systems over convectively active boundary layers. *Quart. J. Roy. Meteor. Soc.*, **113**, 445–467.
- Lee, B. D., C. A. Finley, and R. Wilhelmson, 2000: Simulating deep convection initiation by mesocyclones. *Preprints, 20th Conf. on Severe Local Storms*, Amer. Meteor. Soc., Orlando, FL., 70–73.
- Marquis, J., Y. P. Richardson, and J. M. Wurman, 2007: Kinematic observations of mesocyclones along boundaries during IHOP. *Mon. Wea. Rev.*, **135**, 1749–1768.
- McCarthy, J. and S. E. Koch, 1982: The evolution of an Oklahoma dryline. part I: A meso- and subsynoptic-scale analysis. *J. Atmos. Sci.*, **39**, 225–236.
- McPherson, R. A., C. A. Fiebrich, K. C. Crawford, J. R. Kilby, D. L. Grimsley, J. E. Martinez, J. B. Basara, B. G. Illston, D. A. Morris, K. A. Kloesel, A. D. Melvin, H. Shrivastava, J. M. Wolfenbarger, J. P. Bostic, and D. B. Demko, 2007: Statewide monitoring of the mesoscale environment: A technical update on the Oklahoma mesonet. *J. Atmos. Oceanic Technol.*, **24**, 301–321.
- National Research Council, 1998: *The Atmospheric Sciences: Entering the Twenty-First Century*. National Academy Press.
- Parsons, D. B., M. A. Shapiro, and E. Miller, 2000: The mesoscale structure of a nocturnal dryline and of a frontal-dryline merger. *Mon. Wea. Rev.*, **128**, 3824–3838.
- Rinehart, R. E. and E. T. Garvey, 1978: Three-dimensional storm motion detection by convective weather radar. *Nature*, **273**.
- Roberts, R. D., F. Fabry, P. C. Kennedy, E. Nelson, J. Wilson, N. Rehak, J. Fritz, V. Chandrasekar, J. Braun, J. Sun, S. Ellis, S. Reising, T. Crum, L. Mooney, R. Palmer, T. Weckwerth, and S. Padmanabhan, 2008: Refract-2006: Real-time retrieval of high-resolution low-level moisture fields from operational NEXRAD and research radars. *Bull. Amer. Meteor. Sci.*, **89**, 1535–1548.
- Shimose, K., M. Xue, R. D. Palmer, J. Gao, B. L. Cheong, and D. Bodine, 2009: Two-dimensional variational analysis of near-surface moisture from simulated radar refractivity-related phase change observations. *13th Conf. IOAS-AOLS*, A. M. Soc., ed., volume submitted.
- Stull, R. B., 1988: *An Introduction to Boundary Layer Meteorology*. Kluwer Academic, 666 pp.
- Tuttle, J. D. and G. B. Foote, 1990: Determination of the boundary layer airflow from a single doppler radar. *J. Atmos. Oceanic Technol.*, **7**, 218–232.
- Uccellini, L. W., P. J. Kocin, and J. M. Sienkiewicz, 1999: *Advances in forecasting extratropical cyclogenesis at the National Meteorological Center*. Number 317-336, Amer. Meteor. Soc.
- Weckwerth, T. M., H. V. Murphey, C. Flamant, J. Goldstein, and C. R. Pettet, 2008: An observational study of convection initiation on 12 June 2002 during IHOP 2002. *Mon. Wea. Rev.*, **138**, 2283–2304.
- Weckwerth, T. M., D. B. Parsons, S. E. Koch, J. A. Moore, M. A. LeMone, B. B. Demoz, C. Flamant, B. Geerts, J. Wang, and W. F. Feltz, 2004: An overview of the International H2O Project (IHOP) and some preliminary highlights. *Bull. Amer. Meteor. Sci.*, **85**, 253–277.
- Weckwerth, T. M., C. R. Pettet, F. Fabry, S. Park, M. A. LeMone, and J. W. Wilson, 2005: Radar refractivity retrieval: Validation and application to short-term forecasting. *J. Appl. Meteorol.*, **44**, 285–300.
- Weckwerth, T. M., J. W. Wilson, and R. M. Wakimoto, 1996: Thermodynamic variability within the convective boundary layer due to horizontal convective rolls. *Mon. Wea. Rev.*, **124**, 769–784.
- Ziegler, C. L., T. J. Lee, and R. A. P. Sr., 1996: Convective initiation at the dryline: A modeling study. *Mon. Wea. Rev.*, **125**, 1001–1026.
- Ziegler, C. L. and E. N. Rasmussen, 1998: The initiation of moist convection at the dryline: forecasting issues from a case study perspective. *Wea. Forecasting*, **13**, 1106–1131.